Arab Gulf J. Scient. Res., Math. Phys. Sci., **A6** (3), pp. 439-460 (1988)

Effect of Surface Finish on Microhardness Measurements

Nuri Sabir Mohamed

University of Jordan, Amman, Jordan

ABSTRACT. Vickers microhardness indentations on steel cause deformations in only a small volume of the material. As a result, the values obtained greatly depend on the surface finish in the vicinity of the indentation.

This study investigates the dependence of microhardness test results on the test loads and surface conditions of a BS 970 steel in three heat treatment conditions.

Extensive measurements of the universally accepted roughness average were carried out on different ground and polished metallographic surfaces. Profile graphs were recorded and microhardness measurements carried out under loads of 10, 20, 50 and 100 grams. At low loads, 10g, the measured hardness increased with the degree of polish (*e.g.* with the decrease in roughness average), whilst in hard steel, this effect persists upto 50g load. The shapes of indentations are affected by the directional characteristics of the grinding pattern.

Surfaces used for Vickers microhardness indentations always require metallographic preparation prior to the microhardness testing. Such surface preparation, usually accomplished by mechanical abrading-grinding and polishing, although acceptable for the microhardness test is not completely smooth or scratch-free, Fig. (1).

A satisfactory quantitative evaluation of the texture of such metallographic surfaces was obtained by recording profile graphs, Figs. (2), (3), (4), (5) and (6). These graphs record the vertical heights of surface irregularities and their horizontal spacings at different magnifications. V_v and V_n respectively. The average value of the height of irregularities was also measured as the depth of roughness R_t or the roughness average R_a, in microns, where R_t is generally 7 to 14 times greater than R_a. [3, 8, 9, 10, 11]

Typical values for medium carbon steel surfaces prepared through a standard sequence of grinding and polishing were R_t = 1.5 to 10 um, and R_a = 0.2 to 1.1

um, Figs. (8), (9) and (10). These values of peak to valley heights were larger than the diagonal d of the indentations produced under small loads of 10g, 20g, and 50g, photos (1) and (2), and affect the indentation process by changing the micro-mechanics of metal flow during compression by the Vickers pyramid.

This study investigates how the presence of protruding metal peaks and valleys on the surfaces to be tested affect the magnitude of the pressure on the indenter and the microhardness values.

Indentation Theory

The plastic zone and the flow fields, slip-line fields, beneath the diamond tip penetrating the surface of the metal, calculated [4, 7, 12] are shown in Figs. (11), (12) and (13) which illustrate the situation where the surface peaks are compressed by the facets of the Vickers pyramid such that the apex 0 of the peak (total angle = 2β) is compressed. Let AA' be the contact between the flattened peak and the surface of the Vickers indenter at some moment during the indentation process. In an analysis similar to the method of solution for wedge indentation [7], the apex point 0 moves at 45° to the surface of indenter to point B. Point A is the extreme edge of the metal displaced inwards by the indenter, so AB is the line of contact with the indenter. While the apex of the indenter pyramid is still clear of the lowest point of the adjacent valley, V, point C lies on the surface of the original peak, and AC is a free surface. This requirement, together with the condition that the slip-line meets both the free surface and the indenter surface at 45°, defines the slip-line BDEC. It also determines the angular span ψ of the field ADE. The positions of the displaced surfaces can be solved when AB, AC and the sliplines in ABD and AEC are straight; while ADE is a field of radii and circular arcs. The magnitude of the angle DAE is determined from Fig. (12) as follows:

$$OF = OC \cos(\theta - \beta)$$

$$OF = (OK + CK) \cos(\theta - \beta)$$

$$OF = (OH \sin\theta + AB \cos\psi). \frac{\cos(\theta-\beta)}{\sin(\theta-\beta)} \quad \text{and,}$$

$$GL = GA + AB + BL$$

$GL = (AB(1+\sin\psi) + OH \sin\theta$ also, $OF = GL$, therefore, $OH \sin\theta + AB \cos\psi = AB(1 + \sin\psi) \tan(\theta-\beta) + OH \sin\theta \tan(\theta-\beta)$ and $OH \sin\theta [1-\tan(\theta-\beta)] = AB [\tan(\theta-\beta) + \tan(\theta-\beta) \sin\psi - \cos\psi]$ I

In this equation as the metal peak angle 2β decreases, the angle ψ decreases, and eventually becomes zero when $\tan(\theta-\beta) = 1$, *i.e.* when $\beta = 23°$. Furthermore, negleting work-hardening, the pressure on the surface of the indentor $P_\perp$, is givfn [15] as; $P_\perp = 2K(1+\psi)$. When $\beta = 23°$, $\psi = 0$, the pressure $P_\perp$ reduces to P1 = 2K = the compressive yield stress.

In practice the metal peak angle 2β can be determined from the corresponding peaks on the profile graphs Figs. (5),(6) and (7) according to the equation, [3] tan

$\beta = \frac{Vv}{Vh} \tan \alpha$. It is noticed that for rough metal surfaces Fig. 5, the peaks have spikey appearances *i.e.* 2α approaching zero. This corresponds to small peak angles 2β on the metal surface. While the peaks of the smoother surface in Fig. (6) are less spikey corresponding to an increase in the value of the angle 2β with a decrease in the roughness average value. This indicates that the mean pressure $P_{\perp}$ on the indenter surface increases with a decrease in the roughness average value.

With further penetration of the indenter, the compression of the protruding metal peak in Fig. (12) is continued. Point A on the displaced surface moves towards the vertex P of the indenter and point C moves downwards to V, Fig. (13), and the means pressure on the surface of the indenter becomes,

$$P_{\perp} = 2K\ (1 + \psi) = 2K\ (1 + \frac{\pi}{2} - \theta)$$

This value of the pressure is approximately only 63% of the pressure required to indent a smooth flat surface [15] Fig. (14). At the end of the indentation process in Fig. (13).

$$\psi = \frac{\pi}{2} - \theta \qquad \ldots\ldots \text{II}$$

$A'N = \frac{d}{2}$ = half the diagonal of the resulting indentation and the following equations are obtained from Fig. (13);

$$AB + 2\ OH \sin \theta = \frac{d}{2\sin\theta} \qquad \ldots\ldots \text{III}$$

$$(AB+OH) \tan \theta - R_t (\tan \theta - \tan \beta) \qquad \ldots\ldots \text{IV}$$

Substituting equation II, III and IV into equation I,

$$\frac{2\sin\theta}{d} = \frac{1}{R_t} \left[\frac{1+\cos\theta-\sin\theta\ \tan(\theta-\beta)}{2\sin\theta-2\ \cos\theta-\tan(\theta-\beta)-1}\right] \frac{1}{\sin\theta-\cos\theta\ \tan\beta} \qquad \ldots\ldots\ldots \text{V}$$

Also the Vickers microhardness MH is given by the equation, [1, 5, 14]

$$MH = \frac{2\sin\theta}{d^2} \cdot P \qquad \ldots\ldots \text{VI}$$

taking $R_t = 10R_a$, and $2\theta = 136^{\circ}$ = apex angle of Vickers pyramid, equations V and VI give;

$$MH = \left[\frac{1.4825 - \tan(\theta-\beta)}{0.5788 - 5.5\tan(\theta-\beta)}\right]^2 . PR_a^{-2} \quad \ldots\ldots \text{VII}$$

If β is a function of R_a, for a certain constant load P, equation VII becomes,

$$MH = CR_a^{-2} \quad \ldots\ldots \text{VIII}$$

where C = constant taking logarithms on both sides, equation VIII becomes

$$\log. MH = \log. C - 2 \log. R_a \quad \ldots\ldots \text{IX}$$

Experimental Work

Disc-shaped specimens, 30 mm-diameter, 20 mm-high, were machined from bars of steel BS 970. All specimens were soaked at 880°C; some of these specimens were quenched in oil; (designated steel OQ); a second group were air-cooled; (designated steel N) and a third group were left to cool in furnace; (designated steel A). These heat-treatment sequences were used to achieve a reasonable range of hardness. The specimens were then prepared to different stages in order to produce metallographic surfaces of varying roughness. [6, 13].

The roughness average, Ra, values of the surfaces of the specimens were measured using a Talysurf 10, with 0.8 mm-meter-cut-off. Due to the directional characteristics of the grinding pattern, measurements of the roughness average were made both across and along the direction of scratches (Lay), Fig. (1),(3) and (4).

Microhardness identations were made on each specimen under loads of 10, 20, 50 and 100 grams (photographs (1) and (2) show the shape of these identations). The average diagonals of identations were measured on a filar micrometer. The corresponding microhardness values were obtained from tables calculated according to equation VI.

Results and Discussions

Figs. (8), (9) and (10) show the roughness average and the depth of roughness as a function of particle size of the abrading papers. Figs. (15), (16) and (17) are logarithmic plots of the average microhardness MV_v against the roughness average R_a, for the three groups of steels A, N and OQ. These plots show reasonable agreement with equation IX. The microhardness values measured under the very low load 10 grams increased with decreasing roughness average. Other microhardness values measured under higher loads of 50 and 100 grams show little or no variation with the change in roughness average values except in steel OQ.

The value of the constant in equation IX can evaluated from the logarithmic plots when Ra = 1.0 and $\log_{10} R_a = 0$. The approximate range of values for these constants are; C = 270 − 300 for steel A, C = 380 − 420 for steel N and C = 520 − 600 for steel OQ. The values vary considerably with the hardness of the steels. This may be due to two situations; firstly, most of the peak spacings recorded in the profile graphs are larger than the biggest indentations in the micrographs. (Although it is always possible that a second population of closely spaced peaks and valleys was present but missed by the stylus). Such a situation reduces the probability of peaks being compressed by the surfaces of the vickers indenter. Secondly, the compression of the protruding peaks may not continue to the extent shown in Fig. (13) when the steel is hard. In such situation the angular span is low, $\psi < (\frac{\pi}{2} - \theta)$, and the result is a higher value of the constant C.

Conclusions

1. Steels prepared for microhardness tests show surface irregularities of varying depths.
2. The micro-mechanics of deformation of these irregularities during indentation differ according to the hardness of the steel.
3. Microhardness measurements made under the very low load of 10 grams, are greatly influenced by surface roughness. These effects are considerable in the soft annealed steel A. This is because the penetration depth, P, of the indenter is very shallow. Fig. (18), a plot of P against Ra, shows that the hardness measurement is consistent when the surface is effectively flat *i.e.* $R_a < P$. Therefore, when using very low loads, it is recommended that surfaces should be polished to a specified smoothness, *e.g.* the roughness average must not exceed the depth of identation, $R_a \not> 0.83$ um.
4. On surfaces prepared by routine grinding and polishing, more reliable microhardness values are obtained when indentations are made under loads higher than 50 grams.
5. The directional characteristic of the grinding patterns affects the shape of the indentation, values of R_a is much lower along the lay than across it, therefore, the diamond indentations seem to be extended at right angles to the lay, photograph (2).

References

Almond, E.A., Roebuck, B. and **Gee, M.G.** (1985) Mechanical Testing of Hard Materials, Metals and Materials, **2**(2): 76-82.

Calladine, C.R. (1969) Engineering Plasticity, Pergamon Press, p. 159-195.

Dag.nall, H. (1980) Exploring Surface Texture, Rank Taylor Habson, p. 15-74.

Frank, A. McClintock and **Ali S. Argon** (1966) Mechanical Behaviour of Materials, Addison-Wesley, p. 453.

George E. Dieter (1976) Mechanical Metallurgy, Second Edition, McGraw-Hill, p. 395-398.

Gunter Petzow (1978) Metallographic Etching, Translators from the German Version; **Rosemarie Koch** and **James A. Nelson,** *American Society for Metals,* p. 25-27.

Hill, R. (1950) The Mathematical Theory of Plasticity Oxford, The Clarendon Press, p. 213-254.

ISO (1880-1979) (E), Instruments for the measurement of surface roughness by profile method-contact (stylus) instruments of progressive profile transformation profile recording instruments.

ISO (1879-1981) (E), Instruments for the measurement of surface roughness by the profile method-vocabulary.

ISO (468-1982) (E), Surface roughness-parameters, their values and general rules for specifying requirements.

ISO (1878-1983) (E), Classification of instruments and devices for measurement and evaluation of the geometrical parameters of surface finish.

Johnson, W. and **Mellor, P.B.** (1973) Engineering Plasticity Van Nostrand Reinhold Co. London, p. 494.

Struers Ltd. (1985) Metallographic Preparation of Ductile Materials, *Metals and Materials,* **1**(11): 686-688.

Vickers Microhardness testing instructions, MHT/1B/2, Printed in England, 3/91/HR/0.5.

William, F. Hosford and **Robert, M. Caddell** (1983) Metal Forming, Mechanics and Metallurgy, Prentice-Hall, Inc., p. 193.

(Received 21/07/1987;
in revised form 26/06/1988)

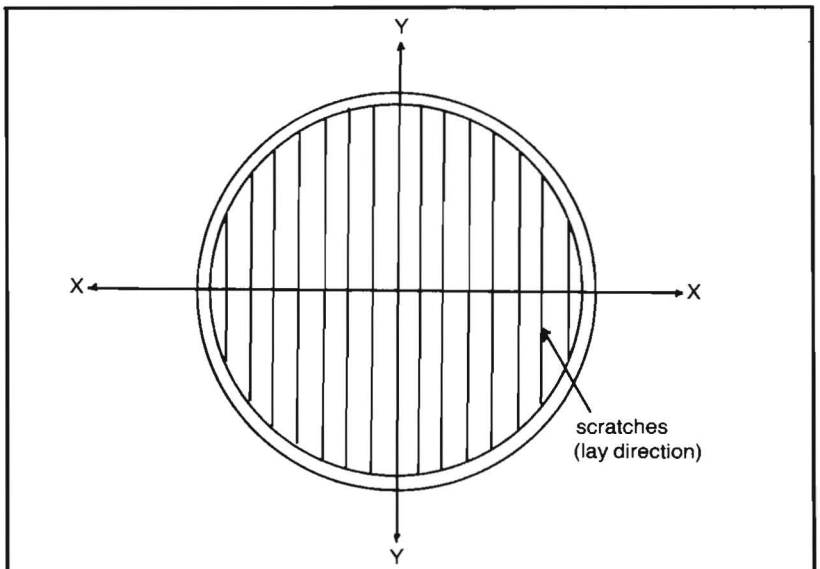

XX measured across the lay.
YY measured along the lay.

Fig. 1. Metallographic surface with scratch-lines produced by mechanical abrading.

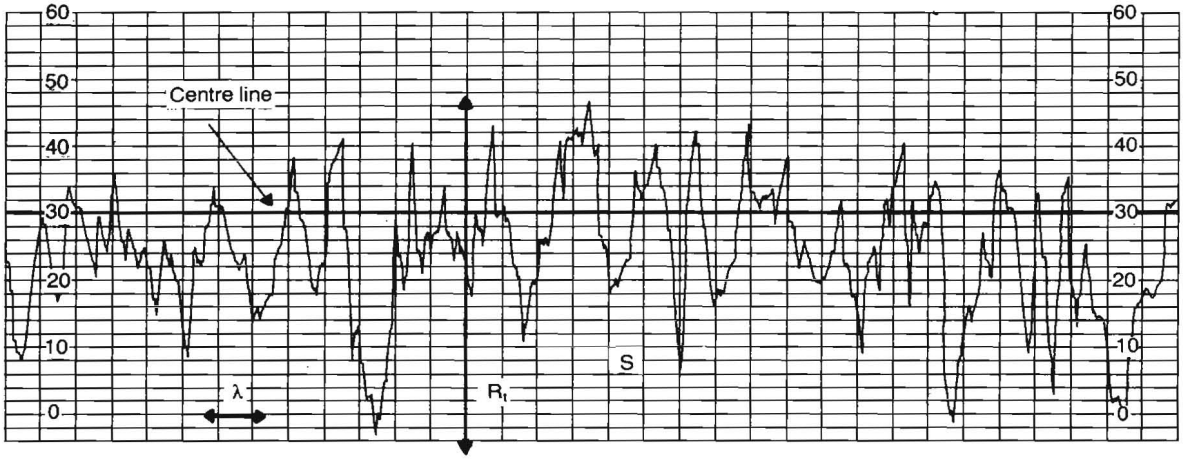

R_t = The depth of rougness, it is the vertical height between the highest and lowest points of the profile within the evaluation length.
S = Peak Spacing
λ_a = Average wavelength; crest spacing.

Fig. 2. Profile graph of a fine-ground surface, normalized specimen, illustration important surface texture parameters. R_a = 1.60 μm, V_v = 5000 X, V_h = 100X.

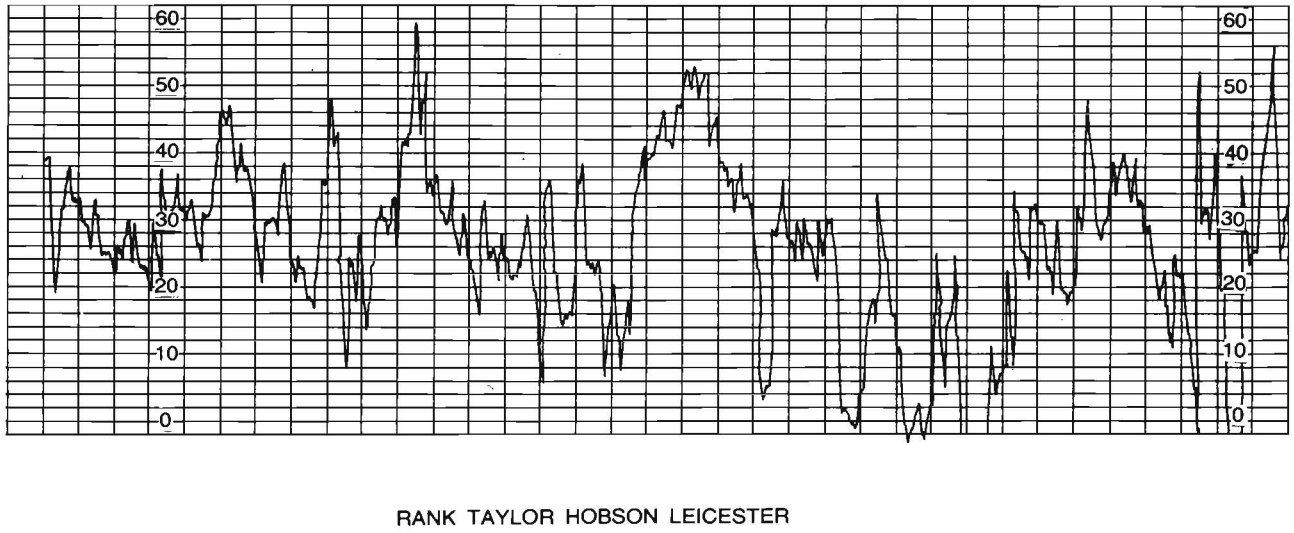

Fig. 3. Profile graph of a ground surface, annealed specimen, measured across the lay centre-line at 30.
R_a = 0.85μm, V_v = 10,000X, V_h = 100X

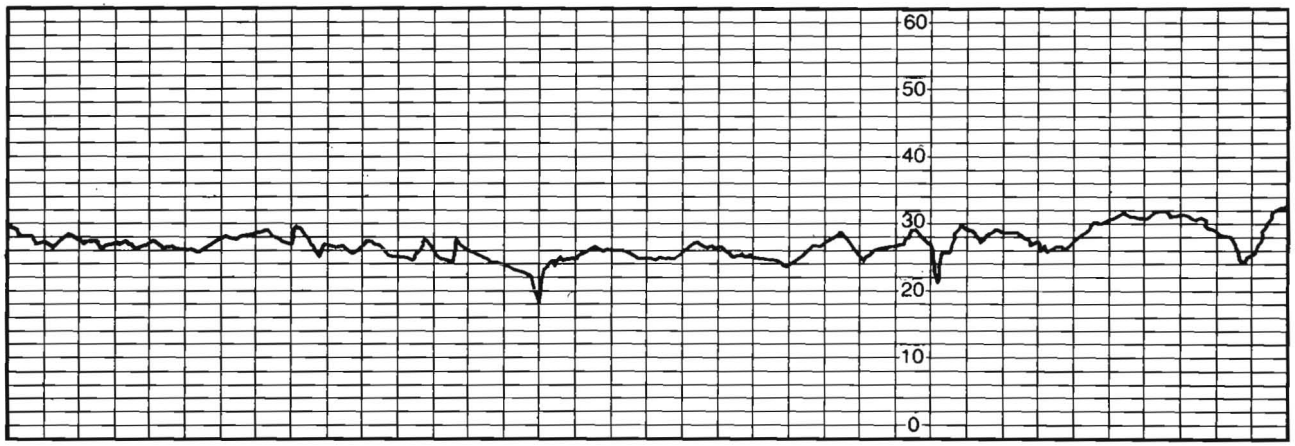

RANK TAYLOR HOBSON LEICESTER

Fig. 4. Profile graph of the same specimen above; but measured along the lay, centre-line at 30. R_a = 0.42μm, V_v = 2000X, V_h = 20X

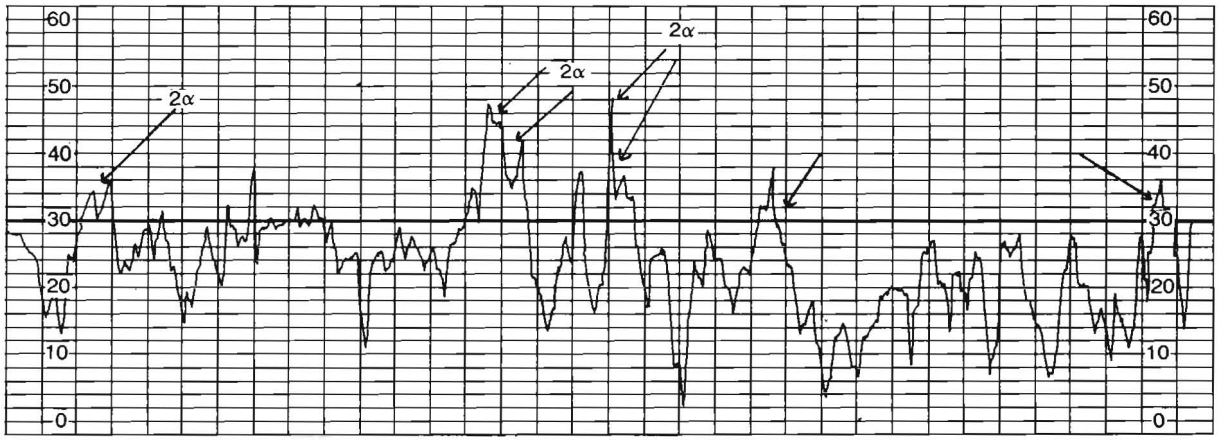

Fig. 5. Profile graph of a fine-ground surface, annealed specimen, R_a = 1.13μm, V_v = 5000X, V_h = 100X centre-line is at 30.
Arrows show protruding metal above centre-line, with Peak angles, (2α).

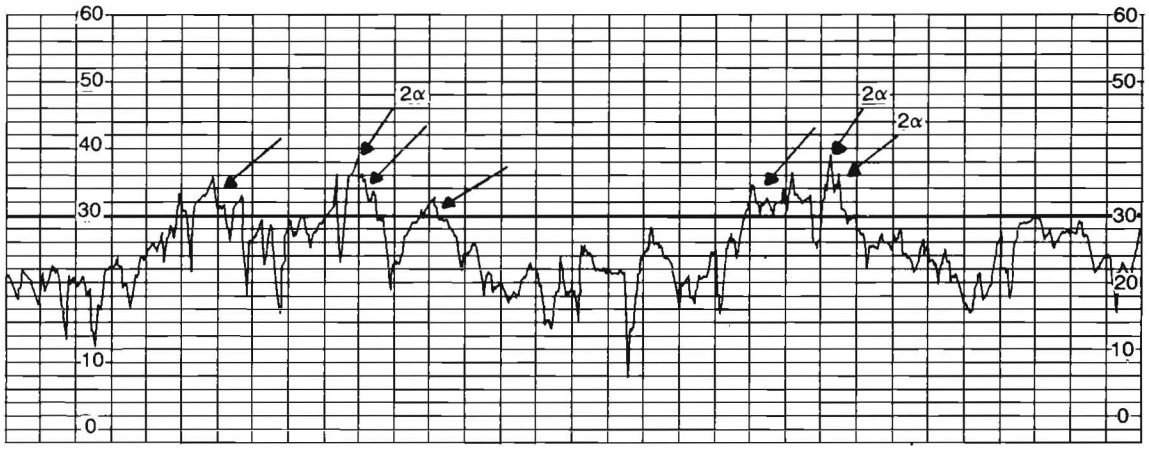

Fig. 6. Profile graph of a fine-ground surface, oil-quenched specimen, $R_a = 0.85\mu m$, $V_v = 5000X$, $V_h = 100X$ centre-line is at 30.
Arrows show protruding metal above centre-line.

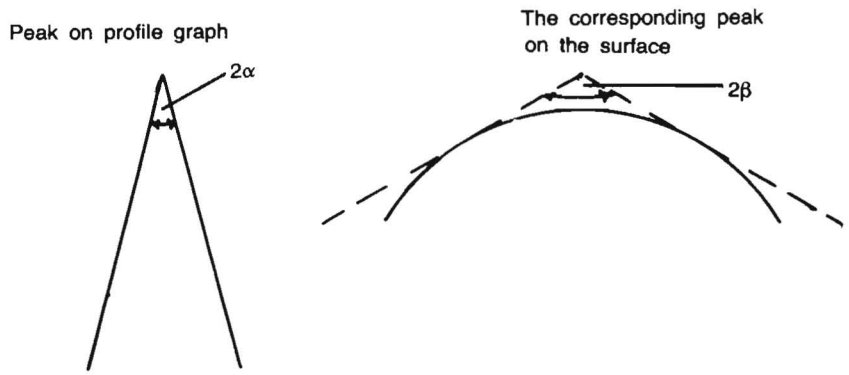

Fig. 7. Relationship between peak angles on the profile graph and the metal surface.

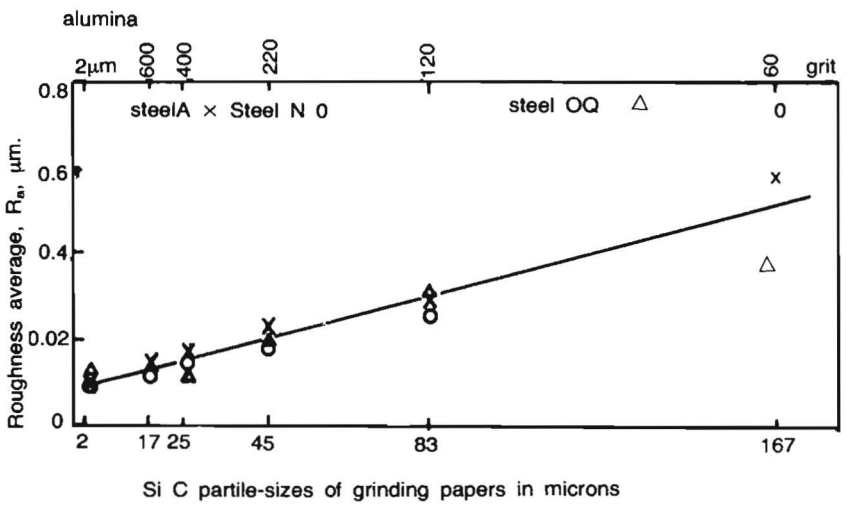

Fig. 8. Roughness measured along lay (Y – Y)

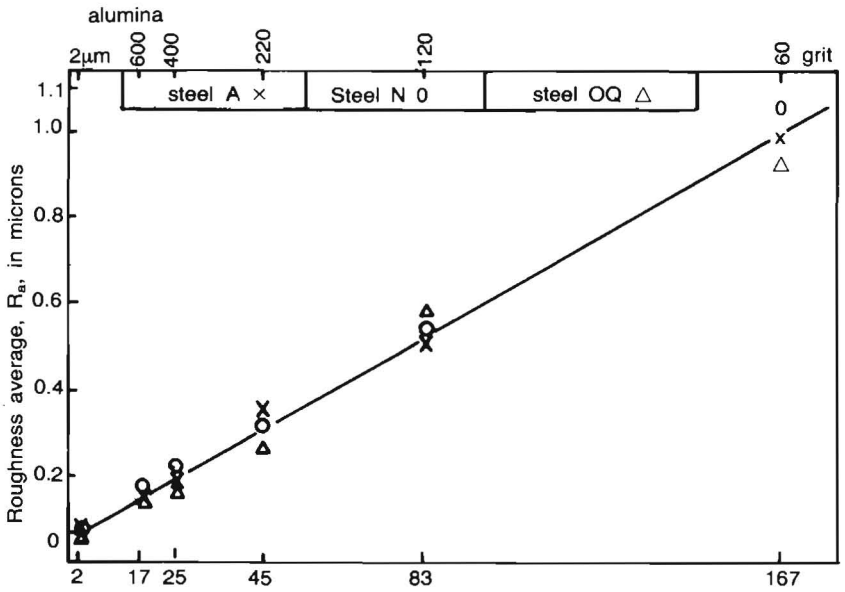

Fig. 9. Roughness measured across lay (X – X)

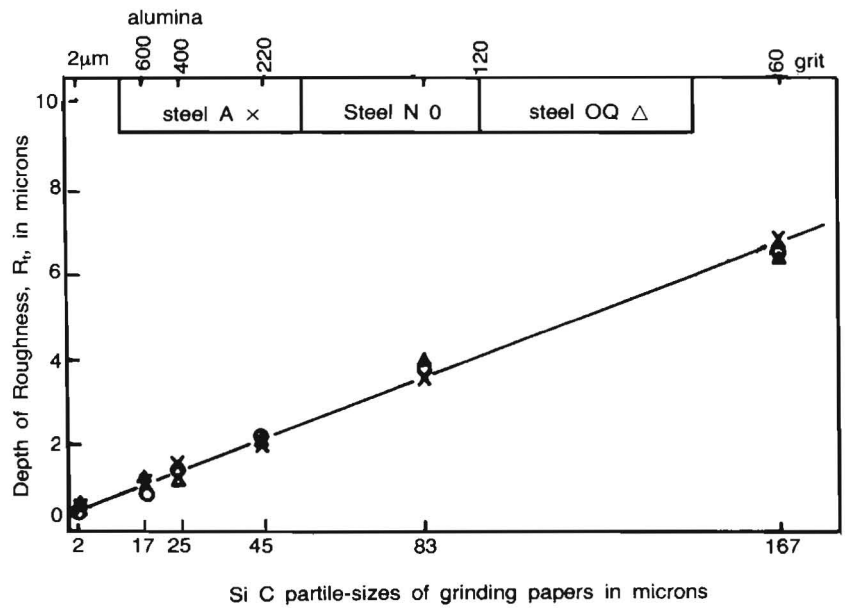

Fig. 10. Roughness measured across lay (X – X)

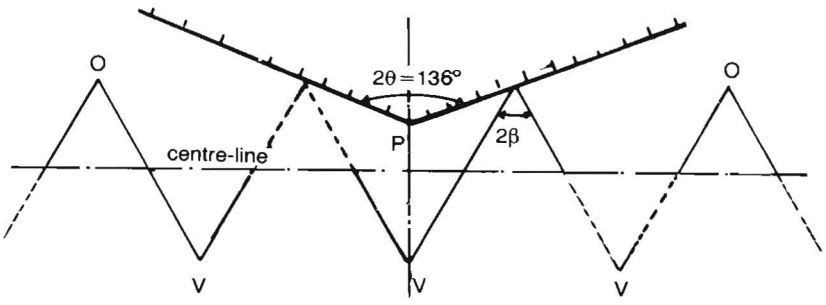

Fig. 11. Symmetrical surface irregularities (peaks, O, valleys V) to be compressed by Vicker's diamond indenter.

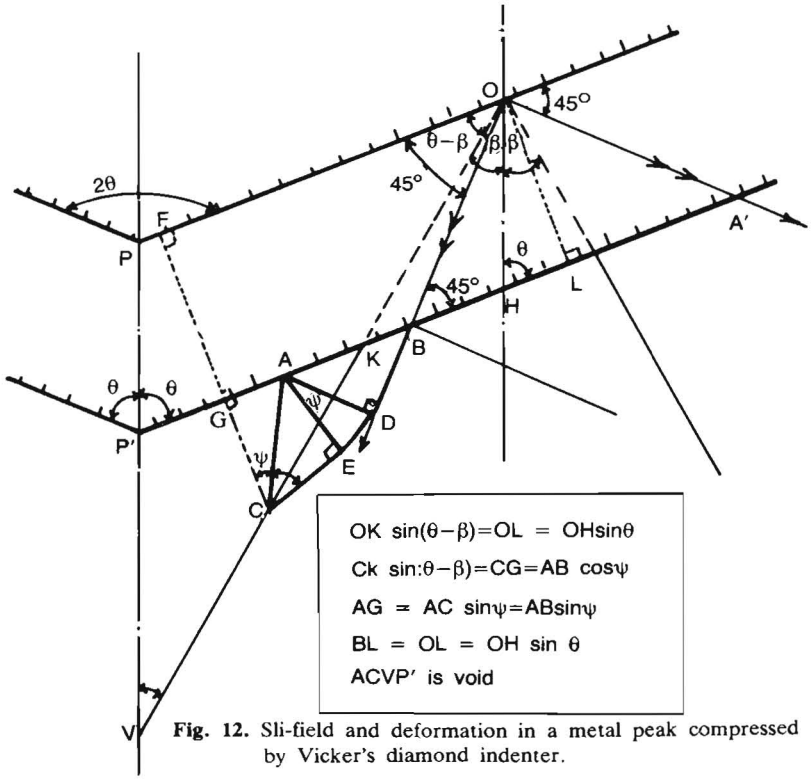

Fig. 12. Sli-field and deformation in a metal peak compressed by Vicker's diamond indenter.

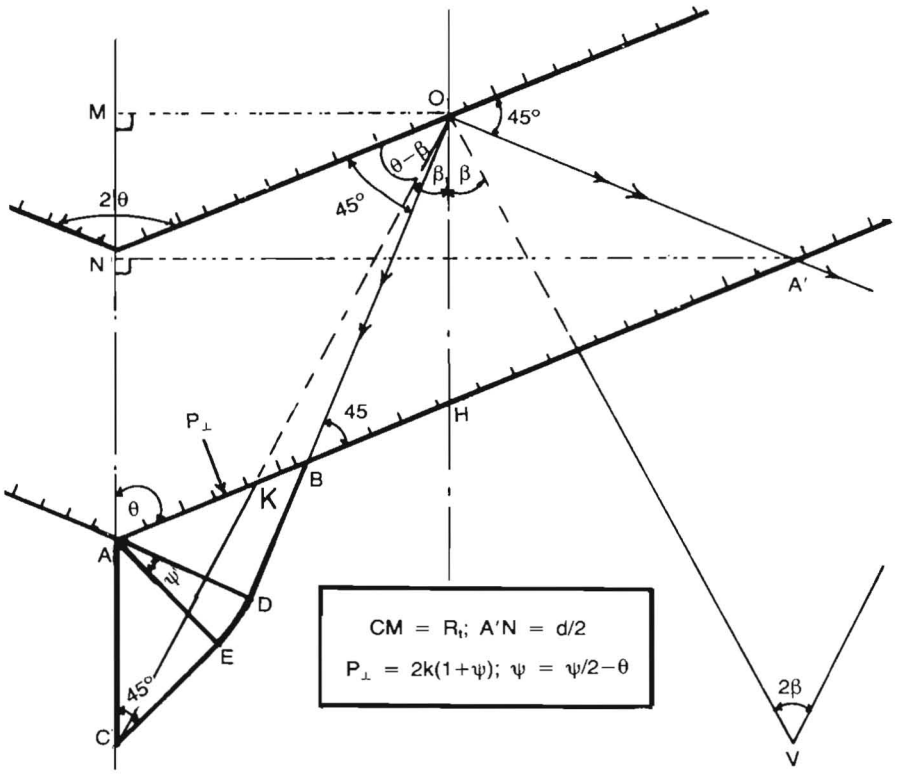

Fig. 13. Sli-line field and deformation of a metal peak O compressed by Vicker's diamond indenter.

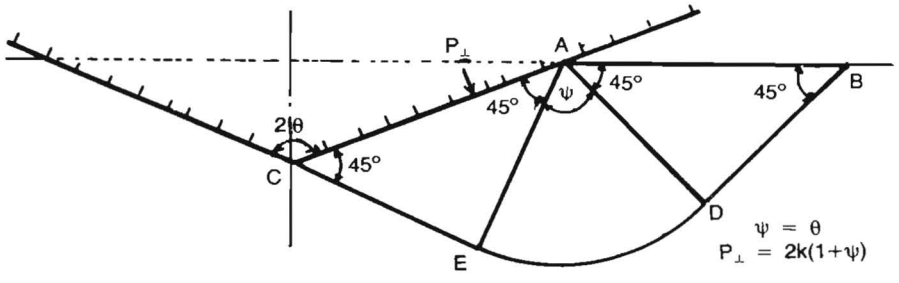

Fig. 14. Sli-line field and deformation of a flat surface indented by Vicker's diamond indenter, no bulging.

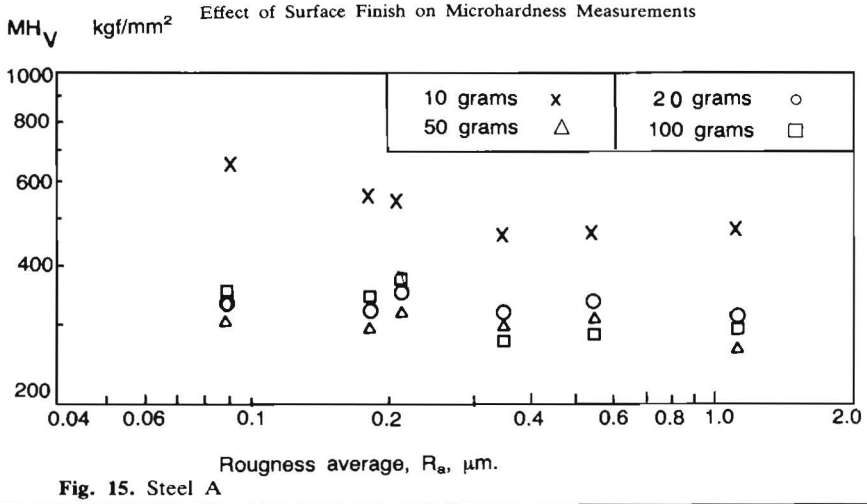

Fig. 15. Steel A

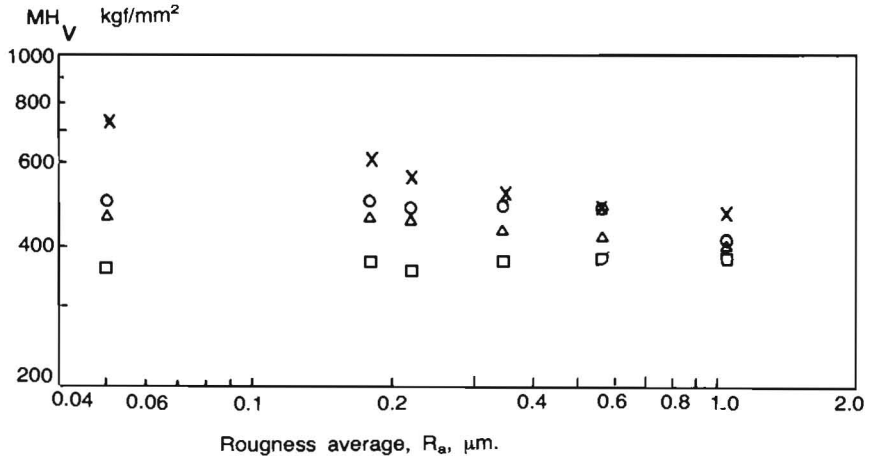

Fig. 16. Steel N

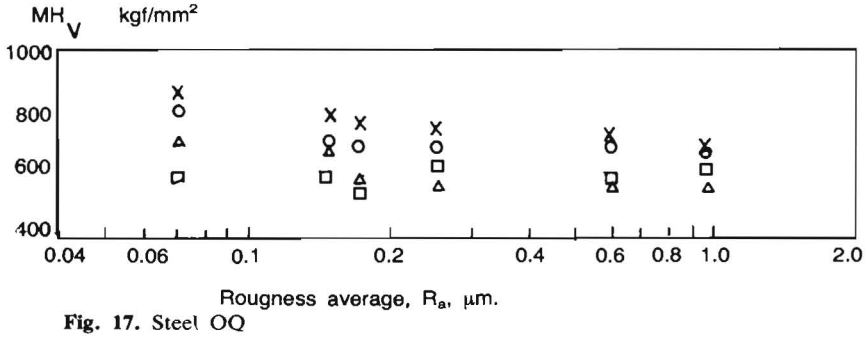

Fig. 17. Steel OQ

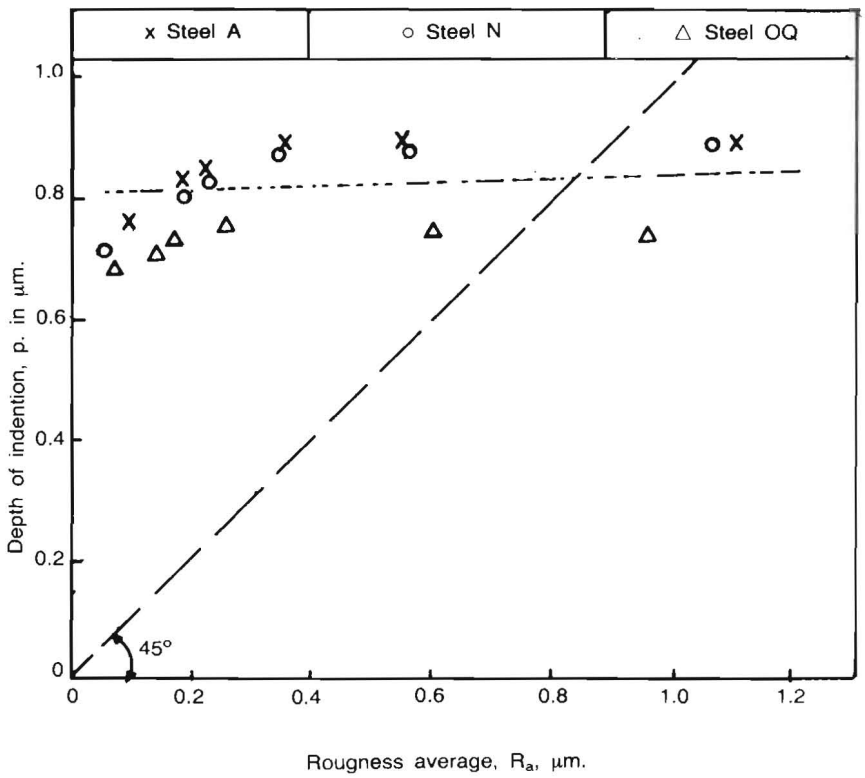

Fig. 18. Depth of indention under load = 10 grams

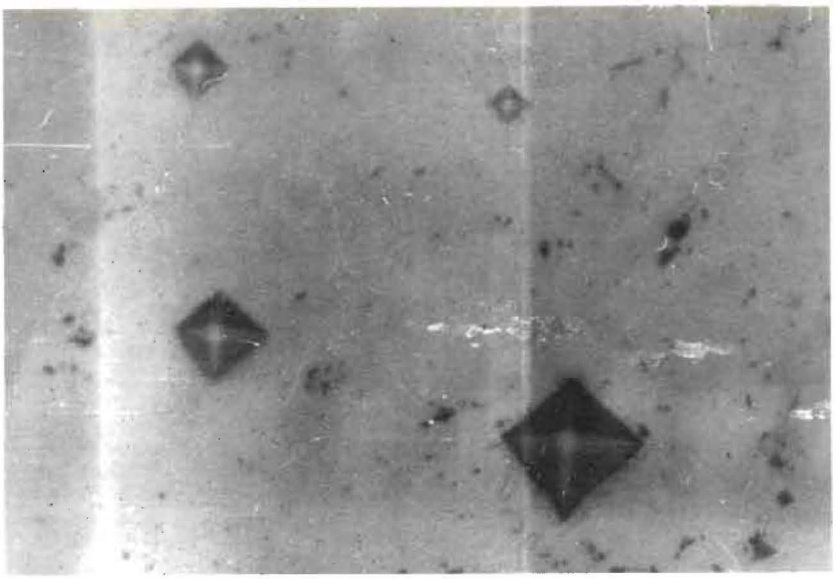

Photo 1. Microhardness indentations on a polished surface of steel N. Magnification 1000x

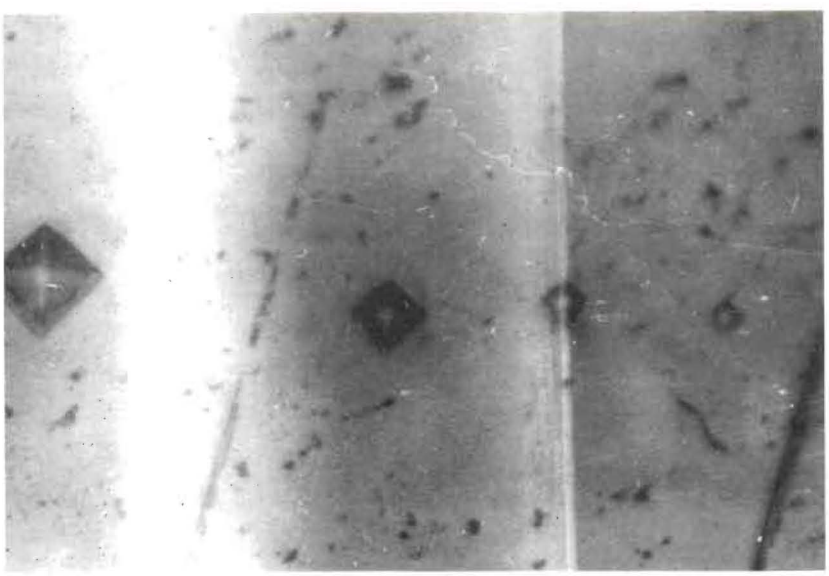

Photo 2. Microhardness indentations on a polished surface of steel OQ. Magnification 1000x

تأثير (أثر) صقل السطح على قياس الصلادة المجهرية

فوزي صابر محمد

الجامعة الأردنية ـ عمان ـ الأردن

يتأثر قياس الصلادة المجهرية كثيراً بنعومة سطح المعدن وخاصة في منطقة اختبار الثلم. ولذلك فإن من المفيد معرفة أثر كل من نعومة الأسطح والأحمال المستخدمة على رقم الصلادة المجهرية.

ويقدم البحث عرضاً مختصراً لبعض النظريات التي تشرح اعتماد التشكيل الدقيق الذي يحدث في اختبار قياس الصلادة. ويتناول بشيء من التفصيل كيفية إنسياب المعدن اللدن تحت ضغط مثلم فيكرز الهرمي الذي يخترق البروز والتموجات (المداميك الدقيقة) الموجودة على سطح المعدن. وقد استخدمت نظريات خطوط الإنزلاق الأساسية من أجل استنباط علاقة بين قيمة الصلادة ودرجة خشونة السطح.

أما عينات التجارب المختبرية فقد تم تحضيرها من فولاذ قياس متوسط الكربون. ووزعت هذه العينات إلى ثلاثة أجزاء أجريت لها معالجات حرارية مختلفة.

وقد أمكن تصليد بعض هذه العينات، وكذلك تجنيس الجزء الثاني لإعطائه صلادة متوسطة.

أما الجزء الثالث والأخير من العينات فقد تم تلدينه إلى صلادة منخفضة بالمقارنة للجزئين السابقين. وتم تحضير كافة العينات للفحص المجهري باتباع مراحل مختلفة من خطوات التجليخ والتلميع لغرض الحصول على أسطح مستوية ذات درجات خشونة متفاوتة.

أجريت قياسات مستفيضة لدرجة خشونة هذه الأسطح وفي اتجاهات متوازية ومتعامدة مع خطوط التجليخ والتلميع. فكانت المرحلة الأولى من هذه

القياسات تخطيط المظهر الجانبي لكل عينة من أجل معرفة شكل النتؤات (المداميك الدقيقة) وعدم الانتظام الموجود على الأسطح المستوية، كما هو موضح بالأشكال من (١) إلى (٦). أما المرحلة الثانية من هذه القياسات فقد اعتمد فيها رقم الخشونة (متوسط الخشونة بالميكرون) والمتبع عالمياً كمعيار كمي لتقييم درجة نعومة أسطح العينات.

وأجريت اختبارات الصلادة الدقيقة بمقياس فيكرز. وتم القياس باختبارات صلادة عديدة للعينة الواحدة وذلك باستخدام أحمال مختلفة، ١٠ جرامات، ٢٠ جراماً، ٥٠ جراماً، ١٠٠ جرام. وكان الغرض منها إحداث كميات اختراق متفاوتة لأداة الاختبار على سطح كل عينة ومن ثم الحصول على أحجام مختلفة للثلم.

ولحساب قيمة (رقم) الصلادة استخدمت الجداول وأيضاً المعادلات الواردة ضمن نظرية الصلادة في متن البحث.

لقد روعي أثناء إجراء التجارب المختبرية أعلاه اتباع المواصفات العالمية المذكورة في المراجع. ويشمل البحث أيضاً نتائج الاختبارات أعلاه على شكل منحنيات أمكن مناقشتها وتحليها. فقد أظهرت النتائج ان شكل الثلم يتغير تبعاً لتغير نسق تجليخ وتلميع أسطح العينات. كما أظهرت هذه النتائج أن الآلية الدقيقة لتشكيل أسطح العينات حول الثلم تختلف تبعاً لصلادة المعدن، ولذلك تتأثر قيمة الصلادة المقاسة تحت أحمال منخفضة كثيراً بخشونة الأسطح.

وقد ازدادت قيمة الصلادة المجهرية مع جودة نعومة الأسطح (أي مع انخفاض رقم متوسط الخشونة) وذلك عند استخدام الأحمال الخفيفة، ١٠ جرامات، ٢٠ جراماً.

والأشكال (١٥)، (١٦)، (١٧) تعطى العلاقة بين رقم صلادة فيكرز ورقم متوسط الخشونة بالميكرون. وقد لوحظ توافق مقبول بين نتائج هذه الأشكال والمعادلة رقم (٩) المستنبطة من التحليل النظري.

ومن أجل تحديد الثوابت والمتغيرات الواردة ضمن المعادلات أمكن تعويض قيم رقم متوسط الخشونة من المنحنيات اللوغاريتمية في المعادلة رقم (٩). ودلت

هـذه الحسابـات على أن قيمـة الثابت في هـذه المعادلـة تزداد مـع زيـادة صـلادة الفولاذ. ويمكن تفسير هـذه الزيـادة بالمقـارنة بـين مخططات المـظهر الجـانبي من الأشكـال (٤)، (٥)، (٦) وبين أحجـام الثلم المختلفـة التي تـظهـر في الصـور الفوتوغرافية.

والشكل (١٨) يدل على أن قيم (رقم) الصلادة تكـون متوازنـة (لا تفاوت فيها) عندما يكون عمق الاختراق أكبر من رقم متوسط الخشونـة، ويحدث ذلـك عند استخدام أحمال عالية (١٠٠ جرام وما فوق).